Néel vector switching and terahertz spin-wave excitation in Mn_2Au due to femtosecond spin-transfer torques

Markus Weißenhofer [1,2,*] Francesco Foggetti [1] Ulrich Nowak [3] and Peter M. Oppeneer [1]

[1]*Department of Physics and Astronomy, Uppsala University, P.O. Box 516, S-751 20 Uppsala, Sweden*

[2]*Department of Physics, Freie Universität Berlin, Arnimallee 14, D-14195 Berlin, Germany*

[3]*Department of Physics, University of Konstanz, D-78457 Konstanz, Germany*

(Received 17 February 2023; accepted 5 May 2023; published 16 May 2023)

Efficient and fast manipulation of antiferromagnets has to date remained a challenging task, hindering their application in spintronic devices. For ultrafast operation of such devices, it is highly desirable to be able to control the antiferromagnetic order within picoseconds—a timescale that is difficult to achieve with electrical circuits. Here, we demonstrate that bursts of spin-polarized hot-electron currents emerging due to laser-induced ultrafast demagnetization are able to efficiently excite spin dynamics in antiferromagnetic Mn_2Au by exerting a spin-transfer torque on femtosecond timescales. We combine quantitative superdiffusive transport and atomistic spin-model calculations to describe a spin-valve-type trilayer consisting of Fe|Cu|Mn_2Au. Our results demonstrate that femtosecond spin-transfer torques can switch the Mn_2Au layer within a few picoseconds. In addition, we find that spin waves with high frequencies up to several THz can be excited in Mn_2Au.

DOI: 10.1103/PhysRevB.107.174424

Konstanzer Online-Publikations-System (KOPS)
URL: http://nbn-resolving.de/urn:nbn:de:bsz:352-2-yjsa4hpn9gwu8

I. INTRODUCTION

Antiferromagnets (AFMs) are promising materials for future spintronic devices. Among the advantages over ferromagnets (FMs) are the faster spin dynamics, the lack of stray fields, the low susceptibility to magnetic fields, and the abundance of materials [1–3]. A challenging aspect in the field of AFM spintronics has been, for decades, the fact that their order parameter is difficult to read and control due to their lack of macroscopic magnetization. Recently, progress was made by the discovery that electrically induced Néel-spin-orbit torques [4] can be used to switch the magnetic order in a certain class of AFMs with broken inversion symmetry, such as CuMnAs [5–7] and Mn_2Au [4,8–13]. An important issue for future device applications is to know in what way, and how fast, such a switching process could best proceed.

A different line of research showed recently that femtosecond laser excitation of a FM creates a burst of spin-polarized current that contributes substantially and in a nonlocal fashion to its ultrafast demagnetization [14–22]. Moreover, it was demonstrated that these spin-current pulses can give rise to an ultrafast spin-transfer torque (STT) [23,24] and excite high-frequency spin waves in an adjacent Fe layer [25,26]. Earlier works have suggested that STTs arising from spin currents transmitted through AFM layers can induce large torques and even switching [27–29]. An intriguing question is what happens when ultrashort spin-current pulses act on an AFM.

Here, we present a quantitative theoretical study to investigate AFM dynamics due to femtosecond STTs emerging from laser-induced demagnetization of a FM. We combine superdiffusive spin-transport calculations and *ab initio* parametrized [12] atomistic spin-dynamics simulations to study a spin-valve-type trilayer consisting of Fe|Cu|Mn_2Au, see Fig. 1(a). Solving numerically the atomistic Landau-Lifshitz-Gilbert (LLG) [30], we demonstrate the formation of thickness-dependent spin-wave spectra with significant peaks at frequencies of up to several THz. Remarkably, we reveal that the laser-induced spin currents can induce Néel-vector switching within 2 ps, opening a pathway for the ultrafast and efficient control of the magnetic order in AFMs.

II. METHODOLOGY

To model the spin current emerging due to the ultrafast laser-induced demagnetization of Fe, we use the superdiffusive spin-transport theory [14] and its extension to magnetic heterostructures consisting of a FM and a nonmagnetic (NM) layer [31]. The model assumes that the laser pulse excites two channels of spin-up and -down electrons, respectively, in the FM layer. Since in the FM layer the two channels have different transport properties (i.e., lifetime and velocities of electrons), the resulting net current is a spin-polarized current which strongly contributes to the femtosecond demagnetization of the FM layer when the current is injected in the NM layer, see Supplemental Material (SM) for details [32].

We model the external laser source S_σ^{ext} that generates the nonthermal electron population as a Gaussian pulse $S_\sigma(E,z) \propto N_\sigma(E,z)\exp\{-\frac{(t-t_0)^2}{2\Delta^2}\}$, where t_0 is the time position of the pulse peak, Δ is the standard deviation of the pulse,

*markus.weissenhofer@fu-berlin.de

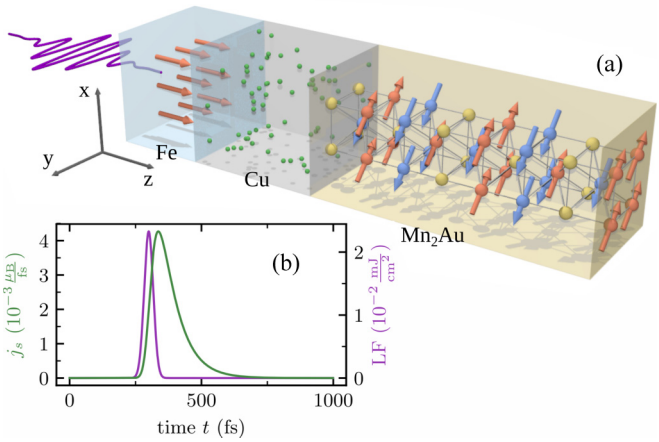

FIG. 1. (a) Sketch of the studied trilayer structure Fe|Cu|Mn_2Au. Magnetic moments are represented by arrows. The Fe layer is excited by an ultrafast laser pulse (purple). The demagnetization of Fe generates a spin current of hot electrons (green balls), which is transmitted through the Cu layer into Mn_2Au, where it exerts a femtosecond STT on the magnetic moments. The two Mn sublattices are illustrated by red and blue spheres and the Au atoms are shown in gold. (b) Laser fluence (LF) of the laser pulse with total fluence of $1\,\mathrm{mJ/cm^2}$ and a FWHM of 40 fs and calculated superdiffusive spin current j_s per atom at the interface between Cu and Mn_2Au. Note that the maximum of the laser pulse is at $t_0 = 300$ fs.

and $N_\sigma(E, z)$ is the number of excited electrons per spin σ in the material. In particular, we assume that the laser has a finite penetration length (λ_{laser}), so the number of excited electrons decays far from the surface $N_\sigma(E, z) = N_0 \exp(-z/\lambda_{\mathrm{laser}})$, and N_0 is a quantity directly proportional to the laser fluence.

Solving the superdiffusive transport equation gives the spin-current density $j_s(z, t)$, shown in Fig. 1(b), which is defined as the difference between spin-up and spin-down electrons flowing in and out at each position z [33].

All results presented below were obtained for laser pulses with full width at half maximum (FWHM) [34] of 40 fs and thicknesses of 16 nm and 4 nm of the Fe and Cu films, respectively. The impact of varying the FWHM on the spin-current pulse and the switching dynamics is discussed in the SM [32].

When the current j_s is transmitted from the Cu layer into Mn_2Au, it exerts a STT [35–37] on the Mn moments. To describe the time evolution of the localized Mn moments under this torque, we numerically solve the LLG equation [30,38]:

$$\frac{\partial \boldsymbol{S}_i}{\partial t} = -\frac{\gamma}{\mu_s}\boldsymbol{S}_i \times \boldsymbol{H}_i^{\mathrm{eff}} + \alpha \boldsymbol{S}_i \times \frac{\partial \boldsymbol{S}_i}{\partial t} + \frac{j_s(z,t)}{\mu_s}\boldsymbol{S}_i \times (\boldsymbol{S}_i \times \hat{\boldsymbol{z}}). \tag{1}$$

$\boldsymbol{S}_i$ are the normalized magnetic moments, $\mu_s = 3.74\,\mu_B$ is the saturation magnetic moment [12], $\gamma = 1.76 \times 10^{11}\,\mathrm{s^{-1}T^{-1}}$ is the absolute value of the gyromagnetic ratio, and α is the dimensionless Gilbert damping parameter. Note that we treat α as a free parameter since no values, neither from experiments nor calculations, are reported in literature. The effective field $\boldsymbol{H}_i^{\mathrm{eff}} = -\partial\mathcal{H}/\partial\boldsymbol{S}_i$ is generated by exchange interaction with neighboring Mn moments and anisotropy terms (see below).

We also consider an additional (third) term due to the femtosecond STT, which acts as an antidamping torque term and is a result of the absorption of the spin current in Mn_2Au [27,29,39]. This term is proportional to the spin-current amplitude j_s of the hot electrons at the interface between Cu and Mn_2Au, the temporal evolution of which we calculate using the superdiffusive spin-transport theory described above. For the setup shown in Fig. 1(a), the polarization of the spin current is along the $\hat{z}$ direction, which is orthogonal to the initial orientation of the Mn moments. It has been demonstrated for FMs that the typical length scale at which spin currents orthogonal to the localized moments are absorbed is at most a few nanometers [25,40,41]. Due to its layered AFM configuration along $\hat{z}$, the propagation of electrons through Mn_2Au can be viewed as electrons passing through an array of FM layers, in each of which some spin momentum is absorbed by the localized Mn moments. We model this by assuming the following spatial profile of the spin current:

$$j_s(z, t) = j_s(0, t)\frac{\exp(-z/\lambda_{\mathrm{STT}})}{\sum_z \exp(-z/\lambda_{\mathrm{STT}})}, \tag{2}$$

where we introduce a penetration depth λ_{STT} [26]. As a general feature of our simulations, we found that larger penetration depths lead to less pronounced peaks in the frequency spectra, as was also demonstrated in Ref. [26], and that they obstruct efficient switching (the latter aspect is also discussed below). Unless stated otherwise, all results presented hereinafter are for $\lambda_{\mathrm{STT}} = 1$ nm, comparable to experimental values [41].

The spin-model Hamiltonian for Mn_2Au we use here has been parameterized in Ref. [12] using *ab initio* calculations and reads

$$\mathcal{H} = -\frac{1}{2}\sum_{i\neq j} J_{ij}\boldsymbol{S}_i \cdot \boldsymbol{S}_j - d_z \sum_i S_{i,z}^2 - d_{zz}\sum_i S_{i,z}^4 - d_{xy}\sum_i S_{i,x}^2 S_{i,y}^2. \tag{3}$$

This Hamiltonian includes exchange between Mn moments at different lattice sites i and j beyond nearest neighbors and the anisotropy terms reflect the tetragonal symmetry of the unit cell. The exchange parameters J_{ij} alternate in sign depending on the distance between the two magnetic moments [12]. The values of the anisotropy constants are $d_z = -0.62$ meV, $d_{zz} = -0.024$ meV, and $d_{xy} = 0.058$ meV. These parameters give rise to a layered AFM ground state where the Néel vectors $\boldsymbol{n}_i = (\boldsymbol{m}_{2i-1} - \boldsymbol{m}_{2i})/2$, with $\boldsymbol{m}_{2i-1/2i}$ being the alternating magnetization (i.e., the sum over the spins in one layer) of the layers along the z axis, are aligned collinearly along the diagonals of the x-y plane (shown in Fig. 1). Given the symmetry of Mn_2Au, the states with the Néel vector along the crystallographic directions [110], [$\bar{1}$10], [1$\bar{1}$0], and [$\bar{1}\bar{1}$0] are equivalent. Note that solving the model used here [42] predicts a critical temperature of 1680 K [12], which is in reasonable agreement with what was reported experimentally [43].

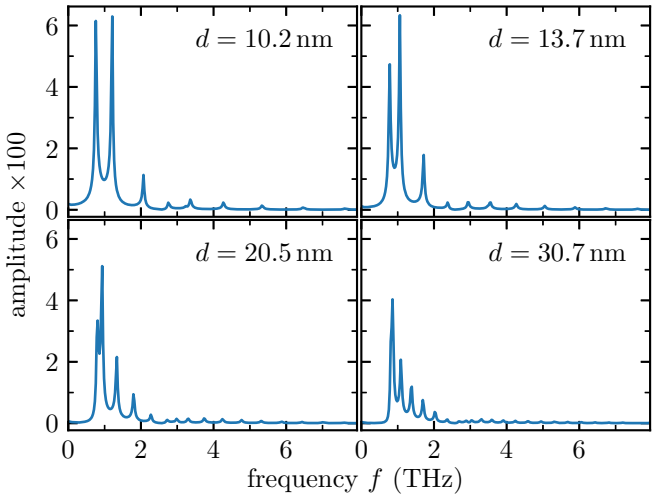

FIG. 2. Amplitudes of excited spin waves (see text) as a function of frequency for different Mn_2Au thicknesses.

III. RESULTS

A. THz spin-wave excitation

To begin, we investigate the formation of standing spin waves (SSWs) that are excited by a laser pulse with an absorbed fluence of $0.24\,\mathrm{mJ/cm^2}$ during the first 40 ps for Mn_2Au layers with thicknesses ranging from 853.9 pm to 30.7 nm. The femtosecond STT excites high-frequency spin waves, which propagate through the Mn_2Au layer and can be reflected multiple times before decaying. We obtain the spectrum of appearing frequencies by performing a Fourier transformation on the time domain of the magnetization in the last layer (note that all spins in the last layer belong to the same sublattice). In Fig. 2, we show the spin-wave frequency spectra for different thicknesses of Mn_2Au. To obtain the amplitude, we calculate the vector length consisting of the absolute values of Fourier transforms of the magnetization in the last layer, i.e., $[|\tilde{m}_x(f)|^2 + |\tilde{m}_y(f)|^2 + |\tilde{m}_z(f)|^2]^{1/2}$ with

$$\tilde{\boldsymbol{m}}(f) = \frac{1}{\sqrt{N_{\mathrm{steps}}}} \sum_{n=0}^{N_{\mathrm{steps}}-1} \boldsymbol{m}_N(t_n) \exp(-\mathrm{i}2\pi f t_n), \tag{4}$$

where N_{steps} is the number of time steps and $t_n = n\Delta t$. The frequency spectra reveal multiple peaks indicating the formation of SSWs of up to several THz. Such high-frequency spin-wave modes have become attractive recently for spintronics operating at THz frequencies [44–46]. The lowest lying peak represents an antiferromagnetic resonance (AFMR) mode and appears for all shown thicknesses at the same frequency of about 0.8 THz. By increasing the thickness d of the Mn_2Au layer, the number of peaks in the displayed range increases since the interval between the peaks decreases (for $d =$ 30.7 nm, the first two peaks even become indistinguishable). This is consistent with the fact that, as a general aspect of standing wave formation, the thickness d of the propagation medium is a multiple of the allowed wavelengths and, henceforth, that the allowed wave vectors scale inversely, i.e., $k_n = n\pi/d$. Since dispersion relations typically feature a monotonic increase in frequency with absolute value of the wave vector, this results in an increased number of peaks within a certain interval for thicker Mn_2Au layers. Note that it is impossible to construct the dispersion relation for spin waves in Mn_2Au solely from the frequency spectra shown in Fig. 2 and the condition for SSW, $k_n = n\pi/d$. This is because the dispersion relation of Mn_2Au has more than one branch, which obstructs the unambiguous identification of the nth peak in the spectrum as belonging to the wave vector k_n (we discuss this in more detail in the Appendix).

Instead, the dispersion relation of Mn_2Au can be obtained using linear spin-wave theory. In the vicinity of the ground state, the Hamiltonian Eq. (3) can be mapped onto a biaxial system with the easy axis along the [110] direction, with an easy axis anisotropy value of d_{xy}, while the hard axis keeps its orientation along the z axis. If only (AFM) nearest-neighbor exchange is assumed, we can use literature formulas for the two emerging AFMR modes [47]:

$$f_0^{\mathrm{a}} = \frac{\gamma}{2\pi\mu_{\mathrm{s}}}[2J^{\mathrm{inter}}d_{xy}]^{1/2} \approx 0.85\,\mathrm{THz}, \tag{5}$$

$$f_0^{\mathrm{b}} = \frac{\gamma}{2\pi\mu_{\mathrm{s}}}[2J^{\mathrm{inter}}(d_{xy}-d_z)]^{1/2} \approx 2.9\,\mathrm{THz}. \tag{6}$$

The effective intersublattice exchange coupling obtained by summing up interactions up to a spatial cutoff of 0.9 nm is given by $J^{\mathrm{inter}} = 371.13$ meV [12]. Albeit the approximations described above, the value for f_0^{a} agrees well with the simulation results. Based on our calculations within linear spin-wave theory, we would expect a second thickness-independent AFMR peak at f_0^{b} in the spectra. However, due to the finite linewidth and the density of the peaks in the vicinity of f_0^{b}, such a peak cannot unambiguously be identified.

B. AFM switching

Upon increasing the laser fluence, the femtosecond STT due to the emerging spin current eventually becomes strong enough to drive the magnetic moments near the interface over the energy barrier induced by the in-plane anisotropy d_{xy}. This excitation propagates through the Mn_2Au layer and can ultimately lead to 90° switching of the Néel vector at the timescale of few picoseconds, see Fig. 3.

This rapid switching is a result of the so-called exchange enhancement, which is characteristic for AFM dynamics [8,12,48–50]. The STT in the LLG Eq. (1) is quadratic in the magnetization and thus has the same direction on each sublattice. This gives rise to a canting between the sublattices and the emerging intersublattice exchange field then leads to a fast precessional motion of the magnetic moments.

Next, we show in Fig. 4 that repeated laser pulses at the same fluence lead to a cyclic switching of the Mn_2Au layer. Each excitation switches the Néel vector by 90° in a counterclockwise direction around the z axis. Note that reversing the polarization of the Fe layer leads to a sign change in the femtosecond STT in Eq. (1) and, hence, to switching in a clockwise direction. The sublattice canting is visible in a small, but finite total magnetization during switching.

Further increase of the laser fluence leads to more canting, so the precessional motion of the magnetic moments close to the interface persists for a longer time. Depending on the timescale of the relaxation back to antiparallel alignment of

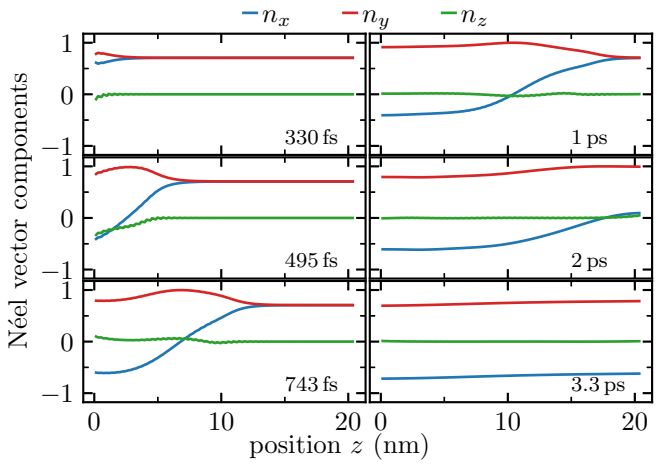

FIG. 3. Components of the Néel vector $\boldsymbol{n}_i$ of Mn_2Au versus distance from the interface to Cu (located at $z = 0$) during the switching process from [110] to [$\bar{1}$10] at different points in time. The laser pulse starts at $t = 0$ and the STT starts at about 300 fs. The absorbed laser fluence has a value of 6.51 mJ/cm^2 and the damping used is $\alpha = 0.01$.

the sublattice magnetizations—which crucially depends on the Gilbert damping parameter α—the rotation of the Néel order parameter can even be larger than 90°. On the other hand, a larger thickness d of the Mn_2Au layer can obstruct the switching because the energy barrier that needs to be overcome scales linearly with d, whereas the total torque due

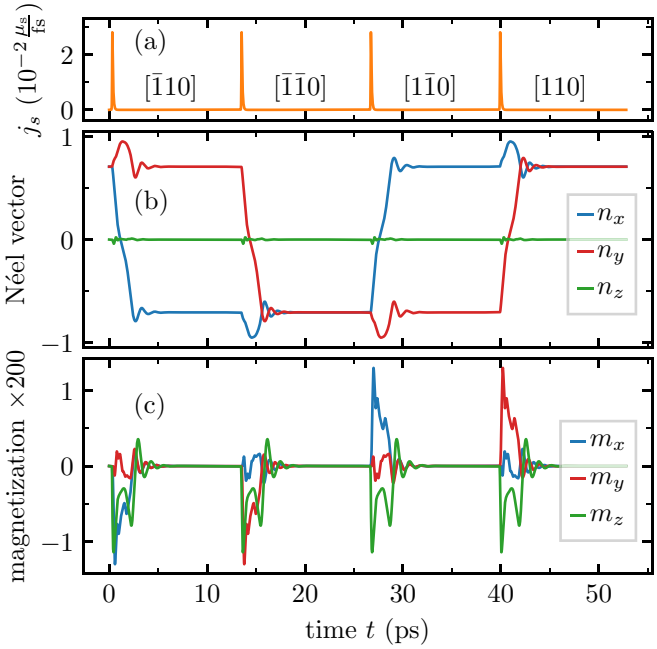

FIG. 4. Cyclic switching of Mn_2Au. (a) Spin current resulting from a sequence of four laser pulses with an absorbed laser fluence of 6.51 mJ/cm^2 every 13.2 ps. (b) Components of the average Néel vector $\boldsymbol{n} = (N/2)^{-1}\sum_{i=1}^{N/2}\boldsymbol{n}_i$, with N being the number of Mn layers. (c) Components of average magnetization $\boldsymbol{m} = (N)^{-1}\sum_{i=1}^{N}\boldsymbol{m}_i$. The system has a thickness of 20.5 nm and the Gilbert damping parameter is set to $\alpha = 0.01$.

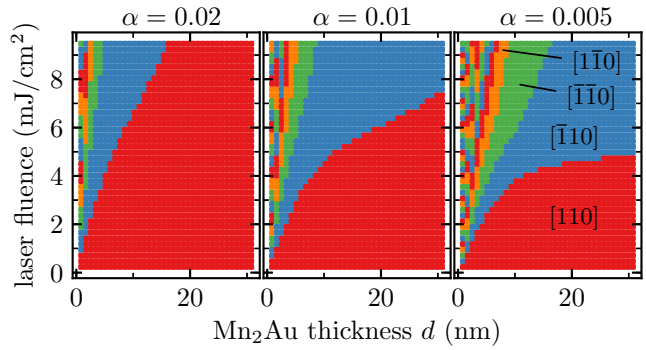

FIG. 5. Switching phase diagram of Mn_2Au due to femtosecond STTs for varying absorbed laser fluences, thicknesses, and values of the Gilbert damping parameter α as labeled. The color coding describes the orientation of the average Néel vector after the laser excitation. Initially, the Néel vector is along the [110] direction.

to the absorption of the spin current close to the interface does not depend on d, as long as d is not comparable to the penetration depth. These features of the switching dynamics are summarized in Fig. 5.

We also want to point out the key role of the highly localized absorption of the spin current in the vicinity of the $CuMn_2Au$ interface. Our results indicate that, in general, larger penetration depths hinder efficient switching, with greatly decreased dynamics in the limit of $\lambda_{STT} \to \infty$, i.e., for spatially homogeneous STT, and much larger fluences are required for switching. As such, describing the switching of AFM layers by ultrafast STT using a two-sublattice macrospin model, as done in Refs. [28,29] for NiO, greatly overestimates the threshold laser fluences as compared to the spatially resolved spin dynamics simulations done here. In addition, our findings indicate that the timescales at which the STTs are present have a decisive impact on the switching threshold: for a constant total laser fluence, higher FWHMs obstruct switching. These aspects are analyzed in more detail in the SM [32].

In Ref. [12], it was demonstrated that thermal activation plays a crucial role in the switching of Mn_2Au via Néel-spin-orbit torques, leading to—in some cases—zero switching probability in the absence of thermal fluctuations and almost deterministic switching at temperatures slightly above room temperature. Here we find, using the stochastic LLG [30], that the temperature enhancement of switching probability is less pronounced; e.g., for $d = 20.5$ nm, $\alpha = 0.01$ and an absorbed laser fluence of 5.68 mJ/cm^2 (which is slightly below the threshold fluence for switching; see Fig. 5), the switching probability only increases up to around 15% at room temperature and to about 35% at 600 K. This difference can be attributed to the fact that here the torques act on the timescale of femtoseconds, in contrast to the 20 ps in Ref. [12]. The impact of temperature on the switching dynamics is discussed in more detail in the SM [32].

IV. CONCLUSION

To summarize, we have studied theoretically the laser-induced excitation of THz spin waves and switching in an

Fe|Cu|Mn_2Au trilayer structure. The spin current emerging from the laser-induced ultrafast demagnetization of Fe was calculated using the superdiffusive spin-transport theory. These spin-current pulses excite spin dynamics in AFM Mn_2Au via femtosecond STTs that were modeled using *ab initio* parametrized atomistic spin-dynamics simulations. Our results reveal the formation of thickness-dependent frequency spectra, demonstrating the formation of SSWs with frequencies of up to several THz. At larger laser fluences, the spin-current pulse leads to ultrafast switching of the Mn_2Au layer. Our quantitative findings predict an efficient way to excite AFMs dynamics—THz spin waves and switching—using trilayer structures and femtosecond laser pulses. As such, they open a pathway for the efficient and ultrafast manipulation of magnetic order in antiferromagnets.

ACKNOWLEDGMENTS

We thank Tobias Dannegger and László Szunyogh for helpful discussions. This paper was supported by the DFG (Deutsche Forschungsgemeinschaft) via TRR 227 Ultrafast Spin Dynamics (Project MF), the Swedish Research Council (VR) (Grants No. 2018-05973 and No. 2021-05211), the K. and A. Wallenberg Foundation (Grant No. 2022.0079), and the European Union's Horizon 2020 Research and Innovation Programme under FET-OPEN Grant Agreement No. 863155 (s-Nebula).

APPENDIX: DISPERSION RELATION OF SPIN WAVES IN Mn_2Au

Spin-wave dispersion relations for arbitrary systems can be efficiently calculated using linear spin-wave theory (LSWT) (see, e.g., Ref. [51]). This approach rests on an expansion of the spin Hamiltonian to second order in the deviations from a reference state, typically the ground state (or any other metastable state).

Here, we map the spin Hamiltonian for Mn_2Au, Eq. (3), onto a one-dimensional biaxial antiferromagnet that extends along the z axis and where only an effective nearest-neighbor exchange is considered. We do this because, for such a system, analytical solutions exist in literature [47].

In the ground state, the Néel vectors of Mn_2Au are oriented along the [110] direction (or any other crystallographically equivalent axis). Thus, as a first step, we rotate the coordinate system by $\frac{\pi}{4}$ around the z axis. In this new basis (indicated by $\sim$), the ground-state Néel vector $\tilde{\boldsymbol{S}}_0$ is parallel to a basis vector; without loss of generality we assume that $\tilde{\boldsymbol{S}}_0 = (\pm 1, 0, 0)^{\mathrm{T}}$. Keeping only terms up to quadratic order in the components orthogonal to the ground state, which we denote by $\tilde{\boldsymbol{S}}_i^{\perp}$, and assuming homogeneity of the spin configuration within the x-y plane, we can map Eq. (3) onto an effective one-dimensional spin Hamiltonian that reads

$$\tilde{\mathcal{H}} = \tilde{\mathcal{H}}_0 - J^{\mathrm{inter}} \sum_{i=1}^{N_{\mathrm{lay}}-1} \tilde{\boldsymbol{S}}_i^{\perp} \cdot \tilde{\boldsymbol{S}}_{i+1}^{\perp} - d_z \sum_{i=1}^{N_{\mathrm{lay}}} \tilde{S}_{i,z}^2 - d_{xy} \sum_{i=1}^{N_{\mathrm{lay}}} \tilde{S}_{i,y}^2, \tag{A1}$$

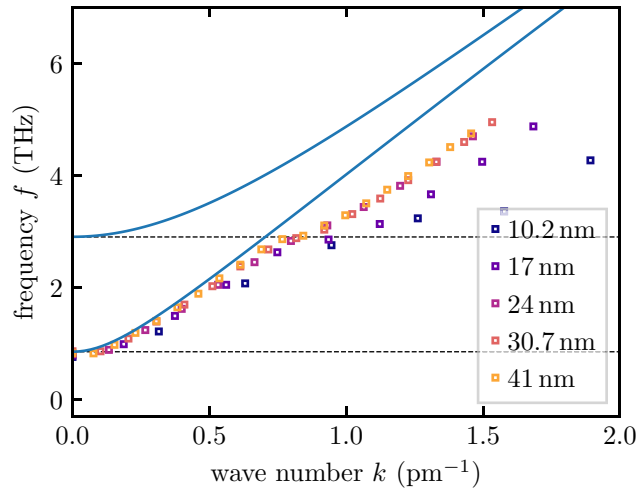

FIG. 6. Spin-wave dispersion relation for Mn_2Au. Solid lines are numerical results obtained using LSWT. Dotted lines are analytical predictions for the two positive AFMR frequencies f_0^{a} and f_0^{b}. The symbols represent the dispersion relation obtained for various Mn_2Au thicknesses using the method described in Ref. [26].

with $\tilde{\mathcal{H}}_0$ being the irrelevant ground-state energy and N_{lay} being the number of Mn layers along the z axis. Note that we have also replaced the long-range exchange interactions with an effective nearest-neighbor exchange. The corresponding exchange constant was calculated in Ref. [12] and has a value $J^{\mathrm{inter}} = 371.13\,\mathrm{meV}$.

The two emergent (positive) AFMR frequencies for this effective spin Hamiltonian, i.e., the spin-wave eigenmodes for which the wave number k is zero, can be calculated using formulas from the literature [47],

$$f_0^{\mathrm{a}} = \frac{\gamma}{2\pi\mu_{\mathrm{s}}}\sqrt{2J^{\mathrm{inter}} d_{xy}} \approx 0.85\,\mathrm{THz}, \tag{A2}$$

$$f_0^{\mathrm{b}} = \frac{\gamma}{2\pi\mu_{\mathrm{s}}}\sqrt{2J^{\mathrm{inter}} (d_{xy} - d_z)} \approx 2.9\,\mathrm{THz}. \tag{A3}$$

For the evaluation of the full spin-wave dispersion we use numerical methods that are explained in detail in the literature, e.g., in Ref. [52]. The two branches of the spin-wave dispersion with positive frequencies close to the Brillouin zone center are shown in Fig. 6 as solid lines. The two dotted lines are placed at the analytical predictions for the AFMR frequencies f_0^{a} and f_0^{b} calculated above.

In Ref. [26], a different approach was used to obtain the spin-wave dispersion relation for Fe. There, the authors also calculated the frequency spectra of spin waves excited by femtosecond spin-transfer torques for varying thicknesses. Using the condition for standing spin waves, i.e., $k_n = n\frac{\pi}{d}$, the authors were able to unambiguously relate the nth peak in the spectrum with the wave number k_n. The spin-wave dispersion for Fe constructed in this way agrees well with analytical predictions based on LSWT. If we follow the same procedure for Mn_2Au, we obtain what is shown as symbols in Fig. 6. While for frequencies below f_0^{b} the dispersion relation obtained this way agrees reasonably well with the results of LSWT—the small deviations could be a result of finite size

effects since they are smaller for larger thicknesses—it is completely off for $f \gtrsim f_0^{\mathrm{b}}$. The reason for this is that above f_0^{b} the peaks in the frequency spectrum could belong to either of the two branches. Moreover, due to the finite linewidth, multiple peaks can overlap, possibly obstructing the unambiguous identification of individual peaks.

[1] T. Jungwirth, X. Marti, P. Wadley, and J. Wunderlich, Nat. Nanotechnol. **11**, 231 (2016).

[2] V. Baltz, A. Manchon, M. Tsoi, T. Moriyama, T. Ono, and Y. Tserkovnyak, Rev. Mod. Phys. **90**, 015005 (2018).

[3] J. Železný, P. Wadley, K. Olejník, A. Hoffmann, and H. Ohno, Nat. Phys. **14**, 220 (2018).

[4] J. Železný, H. Gao, K. Výborný, J. Zemen, J. Mašek, A. Manchon, J. Wunderlich, J. Sinova, and T. Jungwirth, Phys. Rev. Lett. **113**, 157201 (2014).

[5] P. Wadley, B. Howells, J. Železný, C. Andrews, V. Hills, R. P. Campion, V. Novák, K. Olejník, F. Maccherozzi, S. S. Dhesi, S. Y. Martin, T. Wagner, J. Wunderlich, F. Freimuth, Y. Mokrousov, J. Kuneš, J. S. Chauhan, M. J. Grzybowski, A. W. Rushforth, K. W. Edmonds *et al.*, Science **351**, 587 (2016).

[6] K. Olejník, V. Schuler, X. Marti, V. Novák, Z. Kašpar, P. Wadley, R. P. Campion, K. W. Edmonds, B. L. Gallagher, J. Garces, M. Baumgartner, P. Gambardella, and T. Jungwirth, Nat. Commun. **8**, 15434 (2017).

[7] K. Olejník, T. Seifert, Z. Kašpar, V. Novák, P. Wadley, R. P. Campion, M. Baumgartner, P. Gambardella, P. Němec, J. Wunderlich, J. Sinova, P. Kužel, M. Müller, T. Kampfrath, and T. Jungwirth, Sci. Adv. **4**, eaar3566 (2018).

[8] P. E. Roy, R. M. Otxoa, and J. Wunderlich, Phys. Rev. B **94**, 014439 (2016).

[9] S. Y. Bodnar, L. Šmejkal, I. Turek, T. Jungwirth, O. Gomonay, J. Sinova, A. A. Sapozhnik, H.-J. Elmers, M. Kläui, and M. Jourdan, Nat. Commun. **9**, 348 (2018).

[10] M. Meinert, D. Graulich, and T. Matalla-Wagner, Phys. Rev. Appl. **9**, 064040 (2018).

[11] L. Salemi, M. Berritta, A. K. Nandy, and P. M. Oppeneer, Nat. Commun. **10**, 5381 (2019).

[12] S. Selzer, L. Salemi, A. Deák, E. Simon, L. Szunyogh, P. M. Oppeneer, and U. Nowak, Phys. Rev. B **105**, 174416 (2022).

[13] J. Hirst, U. Atxitia, S. Ruta, J. Jackson, L. Petit, and T. Ostler, Phys. Rev. B **106**, 094402 (2022).

[14] M. Battiato, K. Carva, and P. M. Oppeneer, Phys. Rev. Lett. **105**, 027203 (2010).

[15] G. Malinowski, F. Dalla Longa, J. H. H. Rietjens, P. V. Paluskar, R. Huijink, H. J. M. Swagten, and B. Koopmans, Nat. Phys. **4**, 855 (2008).

[16] A. Melnikov, I. Razdolski, T. O. Wehling, E. T. Papaioannou, V. Roddatis, P. Fumagalli, O. Aktsipetrov, A. I. Lichtenstein, and U. Bovensiepen, Phys. Rev. Lett. **107**, 076601 (2011).

[17] D. Rudolf, C. La-O-Vorakiat, M. Battiato, R. Adam, J. M. Shaw, E. Turgut, P. Maldonado, S. Mathias, P. Grychtol, H. T. Nembach, T. J. Silva, M. Aeschlimann, H. C. Kapteyn, M. M. Murnane, C. M. Schneider, and P. M. Oppeneer, Nat. Commun. **3**, 1037 (2012).

[18] A. Eschenlohr, M. Battiato, P. Maldonado, N. Pontius, T. Kachel, K. Holldack, R. Mitzner, A. Föhlisch, P. M. Oppeneer, and C. Stamm, Nat. Mater. **12**, 332 (2013).

[19] B. Vodungbo, B. Tudu, J. Perron, R. Delaunay, L. Müller, M. H. Berntsen, G. Grübel, G. Malinowski, C. Weier, J. Gautier, G. Lambert, P. Zeitoun, C. Gutt, E. Jal, A. H. Reid, P. W. Granitzka, N. Jaouen, G. L. Dakovski, S. Moeller, M. P. Minitti *et al.*, Sci. Rep. **6**, 18970 (2016).

[20] N. Bergeard, M. Hehn, S. Mangin, G. Lengaigne, F. Montaigne, M. L. M. Lalieu, B. Koopmans, and G. Malinowski, Phys. Rev. Lett. **117**, 147203 (2016).

[21] Y. Xu, M. Deb, G. Malinowski, M. Hehn, W. Zhao, and S. Mangin, Adv. Mater. **29**, 1703474 (2017).

[22] A. Alekhin, I. Razdolski, N. Ilin, J. P. Meyburg, D. Diesing, V. Roddatis, I. Rungger, M. Stamenova, S. Sanvito, U. Bovensiepen, and A. Melnikov, Phys. Rev. Lett. **119**, 017202 (2017).

[23] A. J. Schellekens, K. C. Kuiper, R. R. J. C. de Wit, and B. Koopmans, Nat. Commun. **5**, 4333 (2014).

[24] G.-M. Choi, B.-C. Min, K.-J. Lee, and D. G. Cahill, Nat. Commun. **5**, 4334 (2014).

[25] I. Razdolski, A. Alekhin, N. Ilin, J. P. Meyburg, V. Roddatis, D. Diesing, U. Bovensiepen, and A. Melnikov, Nat. Commun. **8**, 15007 (2017).

[26] U. Ritzmann, P. Baláž, P. Maldonado, K. Carva, and P. M. Oppeneer, Phys. Rev. B **101**, 174427 (2020).

[27] H. V. Gomonay and V. M. Loktev, Phys. Rev. B **81**, 144427 (2010).

[28] R. Cheng, M. W. Daniels, J.-G. Zhu, and D. Xiao, Phys. Rev. B **91**, 064423 (2015).

[29] T. Chirac, J.-Y. Chauleau, P. Thibaudeau, O. Gomonay, and M. Viret, Phys. Rev. B **102**, 134415 (2020).

[30] U. Nowak, Classical spin models, in *Handbook of Magnetism and Advanced Magnetic Materials*, edited by H. Kronmüller and S. Parkin (J. Wiley & Sons, New York, 2007), pp. 858–876.

[31] M. Battiato, K. Carva, and P. M. Oppeneer, Phys. Rev. B **86**, 024404 (2012).

[32] See Supplemental Material at https://link.aps.org/supplemental/10.1103/PhysRevB.107.174424 for discussions of (i) the superdiffusive spin-transport model, (ii) the impact of the FWHM and the penetration depth on switching, and (iii) the impact of temperature on switching. This includes a reference to H. Callen and E. Callen, J. Phys. Chem. Solids **27**, 1271 (1966).

[33] W.-T. Lu, Y. Zhao, M. Battiato, Y. Wu, and Z. Yuan, Phys. Rev. B **101**, 014435 (2020).

[34] The FWHM of a Gaussian pulse is related to its standard deviation via FWHM $\approx 2.355\Delta$.

[35] J. Slonczewski, J. Magn. Magn. Mater. **159**, L1 (1996).

[36] L. Berger, Phys. Rev. B **54**, 9353 (1996).

[37] J. C. Slonczewski, J. Magn. Magn. Mater. **247**, 324 (2002).

[38] N. Kazantseva, D. Hinzke, U. Nowak, R. W. Chantrell, U. Atxitia, and O. Chubykalo-Fesenko, Phys. Rev. B **77**, 184428 (2008).

[39] P. Baláž, M. Žonda, K. Carva, P. Maldonado, and P. M. Oppeneer, J. Phys.: Condens. Matter **30**, 115801 (2018).

[40] M. D. Stiles and A. Zangwill, Phys. Rev. B **66**, 014407 (2002).

[41] A. Ghosh, S. Auffret, U. Ebels, and W. E. Bailey, Phys. Rev. Lett. **109**, 127202 (2012).

[42] The numerical integration of the LLG equation is performed using the Heun method [30] with a time step Δt of 0.33 fs. We consider a cross section of $2 \times 2\,\mathrm{nm}^2$ with periodic boundary conditions along x and y directions of the Mn_2Au layer.

[43] V. M. T. S. Barthem, C. V. Colin, H. Mayaffre, M.-H. Julien, and D. Givord, Nat. Commun. **4**, 2892 (2013).

[44] P. Vaidya, S. A. Morley, J. van Tol, Y. Liu, R. Cheng, A. Brataas, D. Lederman, and E. del Barco, Science **368**, 160 (2020).

[45] J. Li, C. B. Wilson, R. Cheng, M. Lohmann, M. Kavand, W. Yuan, M. Aldosary, N. Agladze, P. Wei, M. S. Sherwin, and J. Shi, Nature (London) **578**, 70 (2020).

[46] R. Salikhov, I. Ilyakov, L. Körber, A. Kákay, R. A. Gallardo, A. Ponomaryov, J.-C. Deinert, T. V. A. G. de Oliveira, K. Lenz, J. Fassbender, S. Bonetti, O. Hellwig, J. Lindner, and S. Kovalev, Nat. Phys. **19**, 529 (2023).

[47] S. M. Rezende, A. Azevedo, and R. L. Rodríguez-Suárez, J. Appl. Phys. **126**, 151101 (2019).

[48] C. Kittel, Phys. Rev. **82**, 565 (1951).

[49] E. V. Gomonay and V. M. Loktev, Low Temp. Phys. **40**, 17 (2014).

[50] T. Dannegger, M. Berritta, K. Carva, S. Selzer, U. Ritzmann, P. M. Oppeneer, and U. Nowak, Phys. Rev. B **104**, L060413 (2021).

[51] J. Van Kranendonk and J. H. Van Vleck, Rev. Mod. Phys. **30**, 1 (1958).

[52] A. Donges, N. Grimm, F. Jakobs, S. Selzer, U. Ritzmann, U. Atxitia, and U. Nowak, Phys. Rev. Res. **2**, 013293 (2020).